A proteostasis clock underlies the timing of bacterial dormancy and antibiotic tolerance

Fa-Zhan Wang[1], Yi-Wen Zhang[1,2], and Jia-Feng Liu[1,3]*

[1]Center for Infection Biology, School of Basic Medical Sciences, Tsinghua University, Beijing 100084, China.

[2]Peking University-Tsinghua University-National Institute of Biological Sciences Joint Graduate Program, Academy for Advanced Interdisciplinary Studies, Peking University, Beijing 100871, China.

[3]Tsinghua-Peking Center for Life Sciences, Beijing 100084, China.

*Corresponding authors: Email: jfliu@mail.tsinghua.edu.cn

ABSTRACT

Dormancy, characterized by an extended lag time before resuming growth, protects bacteria from antibiotic stress and facilitates the emergence of resistance. However, a common mechanism that precisely regulates bacterial lag time remains poorly defined. Here we show that the formation and disassembly dynamics of protein aggregates function as a proteostasis clock that governs the lag time distribution. By tracking the aggregate and regrowth dynamics of thousands of cells, we observed that dormant bacteria from diverse genetic and environmental contexts converge to delayed aggregate disassembly as a common rate-limiting step for growth resumption. Mechanistically, the chromosomal replication initiator DnaA is sequestered in aggregates and spatially separated from the nucleoid, thereby preventing DNA replication until proteostasis restoration enables aggregate disassembly. We modulated bacterial lag time distribution by genetically and chemically targeting the proteostasis-replication axis. Remarkably, lag extension scales linearly with the disruption level of proteostasis across diverse backgrounds, indicating a universal coupling between dormancy and proteostasis. This proteostasis collapse renders dormant bacteria, including clinical isolates, more sensitive to additional proteotoxic stress. These findings reveal a timekeeping mechanism in cellular dormancy, highlighting proteostasis as a shared target for combating antibiotic tolerance.

INTRODUCTION

The timing of replication initiation is critical for cells to balance stress tolerance and proliferation[1]. Dormant bacteria exhibit an extended lag time before resuming growth, even upon transition to nutrient-rich environments[2,3]. This growth delay confers protection against antibiotics targeting actively proliferating cells, a phenomenon termed antibiotic tolerance[2-5]. *In vitro* evolution experiments demonstrate that lag duration can be optimized to match the duration of antibiotic treatment, thereby coordinating improved survival and timely regrowth[2]. Increasing evidence establishes lag time as a plastic, heritable, and evolvable trait that facilitates bacterial adaptation to fluctuating environments. Antibiotic tolerance conferred by lag extension impedes the clearance of pathogens during treatment and facilitates the subsequent evolution of resistance[3,6]. Consequently, a better understanding of dormancy regulation is essential for developing strategies to eliminate antibiotic persisters.

Despite numerous mutations extending lag time have been identified in toxin-antitoxin systems[7], aminoacyl-tRNA synthetases[2,3,5], transcriptional regulators[8], and metabolic enzymes[9], it has been a long-standing challenge to determine whether there is a common mechanism underlying these different dormant states. Recent evidence has established a correlation between exit from dormancy and disassembly of protein

aggregates[4,10-12]. Nevertheless, a causal link between protein aggregation and dormancy remains poorly defined, and the specific identity of the aggregate components that govern the lag time distribution has yet to be elucidated[11,12]. We previously reported that the sequestration of seryl-tRNA synthetase (SerRS) into biomolecular condensates regulates compartmentalized translation and bacterial dormancy[13]. However, direct evidence linking the aggregation dynamics of specific proteins to the regulation of the dormancy-proliferation transition remains lacking. More broadly, elucidating the logic of dormancy timing would provide insights into the design principle of timekeeping in biological systems.

To characterize the molecular basis determining the lag time distribution, we integrated automated single-cell lag-time measurements with high-resolution fluorescence microscopy and quantitative omics profiling. Using long-lag mutants of *Escherichia coli*, we observed that increased aggregation of specific proteins, such as the phenylalanyl-tRNA synthetase α subunit (PheS), overwhelmed cellular proteostasis capacity, leading to dose-dependent delays in aggregate disassembly and corresponding increases in lag time. We showed that this aggregate burden delayed replication initiation by stimulating proteases to sequester the chromosomal replication initiation protein DnaA away from the nucleoid. The introduction of aggregates or proteases was sufficient to extend lag time, whereas increasing soluble DnaA levels accelerated dormancy exit, demonstrating a direct proteostasis-replication axis. Across diverse genetic mutants, environmental stresses, and clinical isolates, lag time increased in proportion to the degree of proteostasis disruption, and in turn, accelerating aggregate disassembly through scavenging hydroxyl radicals facilitated dormancy exit. These findings reveal that lag time can be understood as the timescale of cellular recovery from disrupted proteostasis to a replication-competent state. These findings establish cellular proteostasis as a regulating clock that operates in dormant cells.

RESULTS

Long-lag mutants exhibit delayed aggregate disassembly and disrupted proteostasis

To elucidate the regulatory mechanisms governing bacterial lag time, we first performed evolution experiments to identify genetic factors that shape the lag time distribution. Based on the observation that cyclic ampicillin exposure selects for extended lag time[2,3], we evolved *E. coli* KLY under cyclic treatment with the carbapenem ertapenem (ETP). This antibiotic was specifically chosen for the lack of ETP-resistant carbapenemase genes in the KLY strain[2], thus preventing the rapid emergence of resistance and enabling long-term tracking of dormancy evolution. Using ScanLag[14] to quantify single-cell lag time, we observed that, following cyclic ETP treatments, both the mean and variance of colony appearance times increased across three parallel batch cultures (Extended Data Fig. 1a,b). Single colonies exhibiting different lag times were isolated from the evolved lines and analysed by whole-genome sequencing (WGS). Mutations were identified in several aminoacyl-tRNA synthetases (*pheT*, *alaS*, *leuS*) and the cysteine tRNA (*cysT*), each conferring a specific increase in lag time (Fig. 1a and Supplementary Table 1). Notably, two independent mutations were mapped to the phenylalanyl-tRNA synthetase β subunit (*pheT*), both of which produced pronounced lag extension. Restoring the wild-type (WT) allele of *pheT* fully reverted this phenotype (Extended Data Fig. 1c). In line with prior reports implicating multiple aminoacyl-tRNA synthetases (e.g., *metG* and *gltX*) in lag regulation[2,3,5,15], these results hinted at a conserved yet unresolved link between this gene family and dormancy control.

Increasing evidence suggests that protein aggregation facilitates bacterial dormancy, whereas aggregate disassembly is critical for cellular resuscitation[4,11,12]. To examine whether the identified mutants exhibited changed aggregate dynamics, we stained WT and two *pheT* mutants with Proteostat, a fluorescent dye that specifically binds to insoluble protein aggregates[16,17]. Consistent with previous studies[4], we observed the formation of insoluble protein aggregates in stationary-phase (S-phase) bacteria, visible as dark foci in brightfield microscopy and associated with elevated Proteostat fluorescence (Fig. 1b and Extended Data Fig. 1d). However, quantitative analysis revealed that the proportion of cells containing protein aggregates (Fig. 1c) and the intensity of Proteostat fluorescence (Extended Data Fig. 1e) were indistinguishable between stationary-phase WT and *pheT* mutants, despite their markedly different lag times (Fig. 1a). Isolation and quantification of insoluble protein fractions[18] further confirmed comparable levels of aggregated proteins in these strains (Extended Data Fig. 1f). These results indicated that the aggregate amount in stationary-phase cells was insufficient to account for the extended lag time of *pheT* mutants. However, after nutrient replenishment, we observed that WT cells exhibited rapid protein disaggregation within two hours, whereas aggregates in *pheT* mutants persisted for more than six hours until cell division (Fig. 1b,c and Extended Data Fig. 1d,e). Thus, despite the similar aggregate amount, aggregates disassemble more slowly in dormant mutants upon cell resuscitation.

We next determined whether the delayed aggregate disassembly in dormant mutants is merely an epiphenomenon of extended lag time or instead reflects a compromised proteostasis capacity to clear protein aggregates. It is well established that cells with disrupted proteostasis typically exhibit reduced ability to cope with additional proteotoxic stress[19-21]. We compared the sensitivity of WT and *pheT* cells to multiple proteotoxic stressors, including heat shock, oxidative stress, and puromycin, all is known to promote protein aggregation[4,22,23]. Remarkably, killing assays revealed that ETP-tolerant *pheT* mutants were more susceptible to heat shock and hydrogen peroxide than WT cells (Fig. 1d,e). Furthermore, puromycin, an aminoacyl-tRNA analogue that induces misfolded protein accumulation[23,24], caused more pronounced growth inhibition in *pheT* mutants than in WT cells, an effect that was not observed with other antibiotics or non-proteotoxic stressors (Fig. 1f and Extended Data Fig. 2). These results indicate that long lag time confers ETP tolerance but concurrently compromises cellular proteostasis, characterized by delayed aggregate disassembly and increased vulnerability to proteotoxic stress.

Increased PheS aggregation extends lag time in *pheT* mutants

To investigate the molecular basis for the delayed aggregate disassembly in *pheT* mutants, we compared the composition of insoluble aggregates isolated from stationary-phase WT and *pheT* cells. Label-free quantitative proteomics identified phenylalanyl-tRNA synthetase α subunit (PheS) as a top-enriched protein within the aggregates of *pheT* mutants compared to WT cells (Fig. 2a,b). In *E. coli*, phenylalanyl-tRNA synthetase functions as a heterotetramer of two α (PheS) and two β (PheT) subunits, both of which are essential for bacterial viability[25]. Quantitative analysis confirmed that total protein levels of PheS did not increase in both *pheT* mutants, indicating that its increased aggregation results from reduced solubility (Extended Data Fig. 3a,b). To validate these proteomic data, we tagged PheS with ECFP and monitored its spatiotemporal localization during dormancy. We observed the formation of PheS-ECFP aggregates in stationary-phase cells that colocalized with Proteostat signals (Fig. 2c and Extended Data Fig. 3c). Upon nutrient replenishment, these aggregates disassembled rapidly in WT cells but persisted longer in *pheT*

mutants (Fig. 2c and Extended Data Fig. 3c). These results show that in dormant bacteria, *pheT* mutations cause increased accumulation and delayed clearance of PheS aggregates.

To establish a causal relationship between PheS aggregation and dormancy, we examined how titrating PheS levels modulated aggregate dynamics and lag time. Specifically, bacteria carrying an IPTG-inducible PheS-ECFP system were grown for 48h into stationary phase under graded concentrations of IPTG. Quantitative analysis of PheS-ECFP and Proteostat fluorescence showed that increased PheS induction elevated the total aggregate burden in *pheT* mutants (Extended Data Fig. 3d). Crucially, upon nutrient replenishment, this elevated PheS aggregation decreased the aggregate disassembly rates in a dose-dependent manner (Fig. 2d) and led to corresponding extensions of lag times (Fig. 2e and Extended Data Fig. 3e,f). At higher levels of PheS induction, the extended lag phase progressed into a loss of culturability, characterized by a remarkable reduction in colony-forming units (CFUs) (Fig. 2f). Increased PheS expression had no detectable effect on aggregate dynamics or lag time in WT cells (Fig. 2d–f and Extended Data Fig. 3d), underscoring the role of wild-type PheT in maintaining PheS solubility. Consistent with previous results, this PheS-induced extension of lag time further enhanced ETP tolerance but compromised the capacity of *pheT* mutants to cope with proteotoxic stress (Extended Data Fig. 3g,h). Collectively, these results show that modulating the degree of PheS aggregation is sufficient to tune cellular proteostasis and lag time distribution in *pheT* mutants.

Aggregate-stimulated proteases sequester DnaA to delay replication initiation

We next sought to elucidate why increased PheS aggregation suffices to delay the transition from dormancy to replication initiation. Given that chaperones and proteases have been reported to facilitate protein disaggregation and cell resuscitation[4,12,26], we tested whether their overexpression could modulate bacterial exit from dormancy. We found that overexpressing chaperones (DnaK, ClpB) failed to accelerate growth resumption, whereas overexpressing proteases (HslVU, Lon) unexpectedly further delayed dormancy exit (Extended Data Fig. 4a). Microscopy showed that the protease HslU formed aggregates colocalized with PheS-ECFP and exhibited synchronized delayed disaggregation in *pheT* mutants after nutrient replenishment (Extended Data Fig. 4b). However, if the primary role of proteases was to clear protein aggregates, their overexpression would be expected to accelerate, rather than delay, the exit from dormancy. A recent study showed that depletion of the protease Lon abolished the extended lag time in a *metG* mutant[5], supporting the function of proteases in promoting dormancy. Indeed, beyond their role in aggregate clearance, accumulating evidence suggests that proteases also actively target and degrade native proteins involved in cell-cycle regulation[1,26,27]. In *Caulobacter crescentus*, proteases are activated by misfolded proteins to degrade the chromosomal replication initiator DnaA and induce cell-cycle arrest[1]. Given the conserved role of DnaA in replication initiation and its specificity as a protease substrate in *E. coli*[28,29], we next explored whether the aggregate-stimulated proteases might regulate DnaA function during cell-cycle progression.

We constructed chromosomal fluorescent fusions of HslU and DnaA and confirmed that this dual-labelling strategy did not perturb the lag time distribution of WT or $pheT^{D1}$ mutant (Extended Data Fig. 5a). Remarkably, we observed that mCherry-DnaA formed aggregates that colocalized with HslU-ECFP in stationary-phase WT and $pheT^{D1}$ cells (Fig. 3a,b). Upon nutrient replenishment, these aggregates dissolved rapidly in WT cells; in contrast, DnaA persisted in a sequestered state within aggregates for over six hours

161 in the dormant mutant (Fig. 3a,b). As previous research has established that protein aggregates typically
162 localize to nucleoid-free regions owing to macromolecular crowding effects in the nucleoid[30,31], we used
163 DAPI staining to examine the spatiotemporal relationship between DnaA and the bacterial nucleoid. We
164 found that DnaA aggregates maintained a spatial separation from the nucleoid throughout the lag phase,
165 rendering the initiator inaccessible to the chromosomal origin of replication (*oriC*) (Fig. 3a,b). As a result,
166 the integration of DnaA into protein aggregates directly prevents DNA replication until restored proteostasis
167 enables aggregate disassembly.

168

169 **Modulating lag time distribution by targeting the proteostasis-replication axis**

170 To validate this proposed mechanism of dormancy, we reasoned that increasing the abundance of protein
171 aggregates or proteases would further exacerbate DnaA sequestration and delay growth resumption.
172 ScanLag analysis demonstrated that either elevated expression of PheS or HslVU markedly extended lag
173 times in the dormant mutants (Fig. 3c,d). In addition, promoting protein aggregation by the antibiotic
174 puromycin also produced similar lag time extensions (Fig. 3e), indicating that this proteostasis-replication
175 axis can integrate different proteotoxic stresses to determine the timing of dormancy. Furthermore,
176 increased HslVU expression acted synergistically with the *pheT* mutations to cause a dose-dependent
177 reduction in colony-forming capacity despite 3 days of incubation (Fig. 3f). These observations indicate that
178 modulating the level of aggregates and proteases could establish a dormancy continuum spanning from
179 lag time extension to an unculturable state[32].

180 Our findings also raise the possibility that releasing DnaA from aggregate-mediated sequestration may
181 facilitate the exit from dormancy. Guided by prior work showing that fluorescent tag positioning may
182 modulate the localization and activity of DnaA[33,34], we compared the phenotypes of variants with mCherry
183 fused to the amino-terminus, carboxy-terminus, or internal regions of DnaA. Notably, we found that, in
184 stationary-phase cells, the carboxy-terminal DnaA-mCherry exhibited significantly lower aggregation levels
185 compared to other variants (Extended Data Fig. 5b,c). As previously reported[29], overexpressing native
186 DnaA caused pronounced growth defects (Extended Data Fig. 5d) owing to hyper-replication initiation.
187 Strikingly, however, we found that overexpression of the soluble DnaA variant not only accelerated growth
188 resumption in $pheT^{D1}$ cells but also completely abolished the extended dormancy induced by elevated PheS
189 and HslVU levels (Fig. 3g and Extended Data Fig. 5d). This enhanced DnaA solubility is likely attributable
190 to the structural masking of its carboxy-terminal domain, supported by the experiments that fusing a
191 solubility-enhancing Maltose-binding protein (MBP) tag exclusively to the carboxy-terminus produced
192 similar effects (Extended Data Fig. 5e,f). Thus, these findings indicate that bypassing the sequestration of
193 DnaA within protein aggregates can directly promote dormancy exit, underlining a decisive role of DnaA in
194 gating the transition from dormancy to proliferation.

195 Nevertheless, we noticed that overexpressing soluble DnaA failed to accelerate dormancy exit in the $pheT^{D2}$
196 mutant (Extended Data Fig. 5g), implying the existence of additional protease targets beyond DnaA in this
197 specific background. Given that *E. coli* encodes multiple proteases, including HslVU, Lon, ClpP (complexed
198 with ClpX or ClpA), and FtsH[26], we systematically examined how expressing each protease affected
199 dormancy exit of different mutants. We found that, while both *pheT* mutants shared a susceptibility to HslVU,
200 they exhibited specific sensitivity to other proteases: $pheT^{D1}$ bacteria were more sensitive to Lon, whereas
201 $pheT^{D2}$ bacteria showed greater sensitivity to ClpA and ClpX (Fig. 3h). These results imply that bacteria

may rely on multiple, partly redundant proteolytic pathways to coordinate stress responses with DNA replication. Altogether, these results reveal a proteostasis-replication axis that can be targeted to precisely modulate the lag time distribution.

Long-lag phenotypes are associated with disrupted proteostasis across diverse backgrounds

We next addressed whether the regulatory mechanism identified in *pheT* mutants could be generalized to other genetically distinct dormant mutants. We observed that a cysteine tRNA mutant (*cysT*^{D1}) exhibited similarly delayed aggregate disassembly and increased puromycin sensitivity (Extended Data Fig. 6a–d). Quantitative proteomic analysis of the insoluble fractions revealed mutation-specific heterogeneity in aggregate composition across *pheT*^{D1}, *pheT*^{D2}, and *cysT*^{D1} cells (Extended Data Fig. 6e,f). Notably, the ferrichrome-transporting outer-membrane protein FhuA[35] showed significantly elevated aggregation levels across all three dormant mutants (Extended Data Fig. 6e,f). We subsequently demonstrated that inducible FhuA expression alone was sufficient to facilitate dormancy in these mutants (Extended Data Fig. 6g,h). This effect was independent of its canonical role in ferrichrome transport, as a transport-defective FhuA Δ236-248 variant[36] produced a comparable extension of lag time (Extended Data Fig. 6i). Moreover, overexpression of the proteases HslVU and Lon further delayed dormancy exit in *cysT*^{D1} cells (Extended Data Fig. 6j,k). Together, these results indicate that the disruption of proteostasis may represent a shared physiological state of distinct long-lag mutants.

These results prompted us to investigate whether the proteostasis-governed dormancy driven by genetic mutations also extends to aggregates induced by environmental stresses. We first confirmed that both heat shock (49 or 55 °C) and puromycin can induce the formation of protein aggregates in WT cells (Extended Data Fig. 7a). Proteostat staining and ScanLag analysis revealed that exposure to 55 °C for 1 hour resulted in delayed aggregate disassembly and a corresponding extension of lag time in WT cells (Fig. 4a,b). In contrast, treatment at 49 °C for 1 hour, although sufficient to induce aggregates in exponentially growing cells (Extended Data Fig. 7a), had no detectable effect on aggregate disassembly or lag time (Fig. 4a,b). These data imply that the bacterial protein quality-control network can buffer low levels of proteotoxic stress to support timely regrowth, and lag time is extended only when cumulative stress overwhelms cellular proteostasis capacity to clear aggregates. Supporting this view, at the concentration below the minimum inhibitory concentration (MIC), puromycin permitted bacterial growth but extended lag times in a dose-dependent manner (Extended Data Fig. 7b). Following treatment with puromycin above the MIC for varying durations, transfer to antibiotic-free medium revealed a post-antibiotic effect where the lag time increased with the duration of preceding exposure (Fig. 4a–c and Extended Data Fig. 7c). These results suggest a cellular memory of accumulated proteotoxic stress. Similar to dormant mutants, stress-induced long-lag WT cells also showed persistent sequestration of HslU and DnaA within aggregates during dormancy (Extended Data Fig. 7d), indicating the conservation of the proteostasis-replication axis across diverse conditions.

Lag-time extension scales with the degree of proteostasis disruption across stresses

To establish a quantitative relationship between proteostasis disruption and lag-time extension across various stresses, we sought a functional indicator that quantifies the degree of proteostasis disruption under different conditions. Since the formation of protein aggregates mainly represents a cellular response to

243 proteotoxic stress rather than a definitive hallmark of proteostasis collapse (Fig. 4a,b and Extended Data
244 Fig. 7a), we tried to employ the bacterial vulnerability to an exogenous proteotoxic challenge, puromycin,
245 as a functional indicator of proteostasis disruption based on the following observations.

246 First, we have confirmed that puromycin can promote protein aggregation, delay aggregate disassembly,
247 and extend lag time in a dose-dependent manner (Fig. 4a–c and Extended Data Fig. 7a–c). Accordingly,
248 progressive disruption of proteostasis would compromise the cellular capacity to handle puromycin-induced
249 aggregation. Second, we previously found that dormant mutants contained a similar aggregate amount
250 relative to WT cells, but exhibited markedly increased puromycin sensitivity (Fig. 1f and Extended Data Fig.
251 1f), indicating that puromycin sensitivity reflects proteostasis disruption more accurately than the aggregate
252 amount. Third, treatment at 49 °C for 1 hour failed to delay aggregate disassembly, consistent with its
253 unaffected sensitivity to puromycin (Fig. 4a,b and Extended Data Fig. 7e). For comparison, the 55°C
254 treatment slowed aggregate disassembly and increased the sensitivity to puromycin at the same time (Fig.
255 4a,b and Extended Data Fig. 7e). These observations support puromycin sensitivity as a sensitive indicator
256 of proteostasis disruption in bacteria.

257 On this basis, we quantified the level of proteostasis disruption following various stresses by measuring
258 their puromycin sensitivity, calculated as the $\log_{10}$ ratio of CFU on antibiotic-free relative to puromycin plates.
259 Strikingly, we observed that lag time increased in proportion to the degree of proteostasis disruption,
260 regardless of stress type (Fig. 4d). In addition to canonical proteotoxic stresses, prolonged exposure to the
261 antibiotic azithromycin or chloramphenicol similarly compromised proteostasis and extended lag times (Fig.
262 4d). This scaling relation suggests a universal coupling between proteostasis disruption and lag extension
263 of bacteria. The quantitative relationship also extended to the dormant mutants, including the previously
264 described[3] long-lag mutant *metG*^{T} (Fig. 4e). Thus, in bacteria, progressive disruption of proteostasis serves
265 as a tunable timer that governs lag time distribution across diverse contexts. As observed in dormant
266 mutants, stress-induced dormancy conferred increased ETP tolerance while simultaneously sensitizing
267 bacteria to puromycin (Fig. 4f). From a clinical perspective, this disrupted proteostasis could represent an
268 Achilles' heel of dormant bacteria, offering a common target for therapeutic exploitation.

269

270 **Restoring proteostasis accelerates dormancy exit**

271 Once antibiotic stress is removed, rapid growth resumption should confer a significant fitness advantage.
272 We therefore performed evolution experiments to identify genetic factors capable of shortening the lag
273 times of *pheT* mutants. Serial passaging of *pheT* mutants in antibiotic-free LB medium resulted in the rapid
274 evolution of shortened lag times within seven cycles (Extended Data Fig. 8a,b). Reverse mutants were
275 subsequently isolated and analysed by WGS (Extended Data Fig. 8c and Supplementary Table 2).
276 Intriguingly, while these reverse mutations mapped to diverse gene families, restored proteostasis emerges
277 as a convergent hallmark among reverse mutants, manifested as accelerated protein disaggregation and
278 reduced sensitivity to proteotoxic stress (Extended Data Fig. 8d,e). These results underscore proteostasis
279 as a regulatory hub shaping lag time distribution.

280 As delayed aggregate disassembly extends lag time, we reasoned that accelerating aggregate disassembly
281 might facilitate dormancy exit. Increasing evidence indicates that reactive oxygen species (ROS),
282 particularly hydrogen peroxide, can form spontaneously at aggregate interfaces and establish a self-
283 reinforcing feedback loop that promotes aggregation[37,38]. Using the H_2O_2-specific fluorogenic probe Peroxy

284 Orange 1 (PO-1)[39,40], we confirmed that H_2O_2 is enriched in aggregates compared to the cytoplasm (Fig.
285 5a,b). Notably, *pheT*^{D1} cells maintained higher H_2O_2 levels than WT cells throughout dormancy (Fig. 5a,b).
286 Consistently, *pheT*^{D1} cells exhibited elevated sensitivity to Fe^{2+} treatment, which reacts with H_2O_2 via the
287 Fenton reaction to generate more hydroxyl radicals[41] (Extended Data Fig. 9a). To determine if the increased
288 H_2O_2 level contributes to delayed aggregate disassembly, we supplemented the medium with catalase to
289 scavenge H_2O_2[42] and monitored disaggregation dynamics. Remarkably, catalase treatment significantly
290 reduced intracellular H_2O_2 levels in *pheT*^{D1} cells (Fig. 5a,b) and accelerated aggregate disassembly (Fig.
291 5c,d). Accordingly, we observed that the addition of catalases directly facilitated the exit from dormancy
292 (Fig. 5e). Similar promoting effects were obtained with the addition of thiourea, another well-characterized
293 hydroxyl radical scavenger[43] (Extended Data Fig. 9b,c). Beyond dormant mutants, catalase treatment also
294 accelerated bacterial growth resumption from puromycin-induced dormancy (Extended Data Fig. 9d). Thus,
295 scavenging hydroxyl radicals serves as an effective strategy to accelerate aggregate disassembly and
296 promote bacterial dormancy exit.

297

298 **Proteostasis-governed dormancy is observed in clinical isolates**

299 Finally, we extended our analysis to other bacterial species, including the clinical pathogenic isolate
300 *Klebsiella pneumoniae* S837. In this strain, prolonged starvation resulted in a pronounced extension of lag
301 time (Fig. 6a). Through Proteostat staining, we observed the formation of protein aggregates in stationary-
302 phase *K. pneumoniae* cells, and upon nutrient replenishment, aggregates disassembled more slowly in the
303 long-lag clinical isolate S837 compared to the laboratory strain ATCC 43816 (Fig. 6b). These observations
304 confirmed a temporal coupling between dormancy exit and aggregate disassembly in *K. pneumoniae*.
305 Moreover, we found that the introduction of misfolded proteins with puromycin alone was sufficient to extend
306 lag times in both *K. pneumoniae* and the Gram-positive bacterium *Bacillus subtilis* (Fig. 6c), indicating that
307 this proteotoxicity-induced dormancy is not restricted to a single bacterial species. From a clinical
308 perspective, extended lag time in *K. pneumoniae* S837 was associated with increased ETP tolerance (Fig.
309 6d); however, this dormant state also sensitized the pathogen to the proteotoxic stressor puromycin (Fig.
310 6d). These findings suggest that the proteostasis-governed dormancy is a common strategy across
311 bacterial species and implicate the proteostasis network as a potential target for therapeutic intervention
312 against antibiotic persisters.

313

314 **DISCUSSION**

315 The accumulation of protein aggregates is typically linked to cytotoxicity and aging-related diseases in
316 eukaryotes[19-21]. The disassembly of such aggregates is often viewed as too slow to be relevant on
317 physiological timescales[44]. However, our work proposes that the kinetics of aggregate disassembly can be
318 repurposed as a functional timing device in bacteria for fine-tuning lag time to match the duration of stress
319 (Fig. 6e). Conceptually, this proteostasis-governed timing device and canonical circadian clocks driven by
320 transcription-translation feedback loops[45] represent two distinct evolutionary solutions to the problem of
321 temporal control. Circadian clocks provide a stable, cell-autonomous mechanism to synchronize internal
322 physiology with the 24-hour light-dark cycle, whereas the proteostasis clock integrates the history of
323 proteotoxic stress and encodes the timescale from disrupted proteostasis to a replication-capable state.
324 From an evolutionary perspective, while dedicated oscillators are favoured in environments with regular

cycles, a highly tunable timer based on the proteostasis network offers a more economical and flexible solution for bacteria adapting to fluctuating and unpredictable environments.

While protein aggregation has been implicated as a bacterial strategy to facilitate dormancy and antibiotic tolerance[46], the mechanistic link between aggregates and cell-cycle progression has remained elusive. Our results suggest that protein aggregation is not simply a passive process of deposition but actively regulates the spatiotemporal dynamics of the replication initiator DnaA, thereby gating the transition from dormancy to replication. Within this framework, increased aggregation engages proteases to sequester DnaA away from the nucleoid, which delays replication initiation until aggregates are disassembled. Guided by this, bacterial lag time can be precisely tuned by genetically or chemically targeting components of the proteostasis-replication axis. While DnaA is identified here as a critical client, other cell-cycle regulators are probably integrated into this timing device, yet its full regulatory architecture remains to be elucidated. Future *in vitro* reconstitution of the minimal components will be essential to unveil the operating principles of this timekeeping module.

Our work decouples the disruption of proteostasis from the mere presence of aggregates. We show that protein aggregation *per se* represents cellular responses to proteotoxic stresses, rather than a definitive indicator of dormancy. Instead, lag time distribution is determined by the disassembly rate of aggregates, a kinetic parameter that reflects the cellular proteostasis capacity. In bacteria, proteostasis is maintained by an intricate network coordinating protein synthesis, folding, trafficking, and degradation[47]. This systemic nature may explain why long-lag phenotypes are associated with such diverse genetic mutations and environmental factors: these perturbations may represent distinct ways that convergently shift the global proteostasis network away from a replication-competent state. In this view, lag time can be understood as a manifestation of how far the proteostasis network has been driven away from the replication state.

Across *E. coli* and clinical *K. pneumoniae* isolates, starvation-induced extension of lag time confers ertapenem tolerance while simultaneously causing collateral sensitivity to proteotoxic stress, revealing a universal trade-off between dormancy and proteostasis. This trade-off highlights proteostasis pathways as promising targets for the clinical elimination of antibiotic persisters, providing two directions for combating dormant bacteria. One approach is to promote protein disaggregation to accelerate dormancy exit, thereby sensitizing bacteria to antibiotics that target actively proliferating cells. An alternative strategy is to exacerbate proteotoxic stress, which would extend lag time and ultimately drive cells toward a loss of culturability.

Beyond bacteria, protein aggregates have been observed in diverse dormant systems, including yeast[48], oocytes[49], stem cells[17], and cancer cells[50,51]. Despite their well-established function in protein storage, our work hints at an active role of aggregates in regulating cell-cycle progression. The evolutionary conservation of the proteostasis network and DNA replication raises the possibility that regulated proteostasis may represent a broader design principle for timekeeping in cellular dormancy.

361 **METHODS**

362 **Bacterial strains, plasmids, and growth conditions**

363 All strains used in this study are indicated in Supplementary Table 3, plasmids in Supplementary Table 4,
364 and primers in Supplementary Table 5. *K. pneumoniae, B. subtilis, E. coli* KLY, and derivative strains were
365 grown at 37 °C in Luria-Bertani (LB) broth (Miller formulation; 10 g/L NaCl, 10 g/L tryptone, and 5 g/L yeast
366 extract) with 220 rpm shaking or on solid LB medium prepared by supplementing the broth with 15 g/L agar,
367 unless otherwise stated.

368 Polymerase chain reaction (PCR) amplification was performed using PrimeSTAR Max DNA Polymerase
369 (Takara) according to the manufacturer's instructions. For plasmid construction, the gene PCR product was
370 amplified from *E. coli* KLY and inserted into the pET28a/pET28a-mCherry backbone using the ClonExpress
371 II One Step Cloning Kit (Vazyme). Cells were plated on LB plates containing kanamycin (100 μg/mL) for
372 selection. Positive clones were validated by Sanger sequencing.

373 To label HslU and DnaA with fluorescent proteins on the chromosome, we used a two-step λ Red
374 recombineering. At the first step, the *kan::sacB* cassette was amplified and transformed into the
375 electrocompetent *E. coli* KLY cells with induced Red protein with IPTG (pSC101-RED-tet). Cells were plated
376 on LB plates containing kanamycin (100 μg/mL) for selection. At the second step, the *hslU/dnaA-*
377 *ECFP/mCherry* translational fusion fragment was amplified, transformed, and recombined into the bacterial
378 genome of the electrocompetent cells with *kan::sacB* cassette at the targeting site and induced Red protein
379 with IPTG, then the cells were counter-selected on sucrose plates. Positive clones were validated by
380 Sanger sequencing. To restore the WT alleles of *pheT* mutants, P1 phage (ATCC 25404-B1) was used to
381 conduct general transduction[52], and primer design was using Dup-In[53].

382

383 **Evolutionary protocol**

384 For antibiotic evolution, an overnight culture was diluted 1:100 into 1 mL LB medium supplemented with 1
385 μg/mL ertapenem and incubated for 4 or 12 hours alternately at 37 °C with shaking. After killing, the cultures
386 were washed twice with 0.9% NaCl to remove antibiotics, resuspended in 1 mL fresh LB medium, and then
387 grown overnight at 37 °C with shaking.

388 For reverse evolution, an overnight culture of dormant mutant was diluted 1:100 into 1 mL antibiotic-free
389 LB medium and grown overnight at 37 °C with shaking.

390

391 **ScanLag analysis**

392 Bacteria were serially diluted to approximately 200 CFU per plate and plated on solid LB medium. The
393 plates were then placed in a ScanLag setup[14] at 37 °C. This setup automatically monitors colony growth
394 every 20 minutes and extracts the distribution of appearance times. The colony detection threshold size is
395 set at 100 pixels.

396

397 **Whole genome sequencing**

398 Genomic DNA was extracted using a TIANamp Bacteria DNA Kit (TIANGEN; Beijing; China). Sequencing
399 was performed by Sinobiocore using Illumina-HiSeq with 150 bp paired-end at an average coverage of 100-
400 200. Single nucleotide polymorphisms (SNPs) and indels were identified by bwa version 0.7.18.

401

402 **Cell staining and microscopy**

403 For Proteostat staining, bacteria were processed following the manufacturer's instructions (Enzo Life
404 Sciences; enz-51035-K100): Briefly, bacteria were fixed with 4% PFA for 30 minutes at room temperature
405 and permeabilized in Assay Buffer with 0.5% Triton X-100 for 30 minutes on ice. Cells were then washed
406 twice with PBS and stained with Proteostat dye for 30 minutes at room temperature. The stained cells were
407 washed twice with PBS before imaging.
408 For DAPI staining, fixed cells were stained with DAPI (MCE, HY-D0814) at a concentration of 1 μg/mL in
409 PBS for 10 minutes at room temperature. The stained cells were washed twice with PBS before imaging.
410 For Peroxy Orange 1 (PO-1) staining, bacteria were stained with PO-1 (MCE, HY-103469) at a
411 concentration of 10 μM in PBS for 1 hour at 37 °C. The stained cells were washed twice with PBS before
412 imaging.
413 Brightfield and fluorescence images were captured using a FV3000 confocal microscope (Olympus) with a
414 100 × objective. Appropriate filter sets were chosen for each fluorophore based on their excitation and
415 emission spectra. All images were analyzed using Fiji.
416

417 **Insoluble protein isolation**

418 The isolation of insoluble proteins was modified from Tomoyasu[16]. Briefly, cells (1 mL, 2×10^9 bacteria)
419 were collected and incubated in 40 μL buffer A (10 mM potassium phosphate buffer, pH 6.5, 1 mM EDTA,
420 20% (w/v) sucrose, 1 mg/mL lysozyme) for 30 minutes on ice. Cells were then mixed with 360 μL buffer B
421 (10 mM potassium phosphate buffer, pH 6.5, 1 mM EDTA) and lysed by sonification while cooling. Intact
422 cells were removed by centrifugation (2000 g, 20 minutes, 4 °C). The insoluble cell fraction was isolated by
423 centrifugation (15000 g, 20 minutes, 4 °C). The pellet fractions were resuspended in 400 μL buffer B with
424 2% NP40 to dissolve membrane proteins and isolated by centrifugation (15000 g, 30 minutes, 4 °C). NP40-
425 insoluble pellets were washed twice with 400 μL buffer B and resuspended in 100 μL buffer B by brief
426 sonification. The concentration of insoluble protein is determined using the BCA protein assay kit
427 (Beyotime).
428

429 **Killing assays**

430 For ertapenem and H_2O_2 killing, bacteria were diluted 1:100 into LB medium supplemented with 1 μg/mL
431 ertapenem or 10 mM H_2O_2 and incubated for the indicated time at 37 °C with shaking. For heat killing,
432 bacteria were diluted 1:100 into LB medium and incubated for 30 minutes at 55 °C. The CFUs were
433 evaluated by plating before and after stress exposure.
434

435 **Culturability tests**

436 Tenfold dilutions of bacteria were prepared in PBS and subsequently plated on solid LB medium
437 supplemented with the indicated concentrations of puromycin or IPTG. The CFUs were calculated after 72
438 hours of incubation at 37 °C.
439

440 **Growth curves**

441 Bacteria were diluted to 2×10^5 cells/mL in a 96-well plate of LB medium. Growth measurements were
442 performed by incubating the plate in a SPARK multimode microplate reader (Tecan) at 37 °C with
443 shaking. OD_{600} was measured every 10 minutes.
444

445 **Quantitative proteomics**
446 The total protein of bacteria is extracted using the Bacterial Protein Extraction Kit (Sangon). The insoluble
447 protein is isolated as previously mentioned. The proteins were separated by SDS-PAGE, respectively. The
448 gel bands of interest were excised from the gel, reduced with 5 mM of DTT, and alkylated with 11 mM
449 iodoacetamide, which was followed by in-gel digestion with sequencing grade modified trypsin at 37 °C
450 overnight. The peptides were extracted twice with 0.1% trifluoroacetic acid in 50% acetonitrile aqueous
451 solution for 30 min and then dried in a speedvac. Peptides were redissolved in 20 μL 0.1% trifluoroacetic
452 acid, and 6 μL of extracted peptides were analyzed by Thermo Scientific Orbitrap Exploris 480.
453 For LC-MS/MS analysis, the peptides were separated by an 85-min gradient elution at a flow rate of 0.30
454 μl/min with a Thermo-Dionex Ultimate 3000 HPLC system, which was directly interfaced with a Thermo
455 Scientific Orbitrap Exploris 480 mass spectrometer. The analytical column was a home-made fused silica
456 capillary column (75 μm ID, 350 mm length) packed with C-18 resin (1.9 μm, Dr.Maisch GmbH). Mobile
457 phase consisted of 0.1% formic acid, and mobile phase B consisted of 80% acetonitrile and 0.1% formic
458 acid. Orbitrap Exploris 480 mass spectrometer was operated in the data-dependent acquisition mode using
459 Xcalibur 4.5.445.18 software, and there was a single full-scan mass spectrum in the orbitrap (350-1600
460 m/z, 60,000 resolution) followed by 2 seconds data-dependent MS/MS scans in an Ion Routing Multipole
461 at 30 normalized collision energy (HCD).
462 The MS data were analyzed using the MaxQuant algorithm (v.2.4.9.0). Spectra were searched against the
463 *E. coli* K12 protein sequences in the Uniprot database. The global false discovery rate (FDR) cutoff for
464 peptide and protein identification was set to 0.01. The label-free quantification (LFQ) algorithm in MaxQuant
465 was used to compare samples.
466 Proteomics statistical analysis was performed using the Perseus algorithm (v.2.0.11.0). LFQ intensities for
467 the protein group table were uploaded to Perseus. Protein groups were filtered to retain only proteins with
468 at least 2 valid values in at least one group. Missing values were replaced from a normal distribution (width
469 = 0.3, down shift =1.8). To compare protein intensities, a *t*-test was performed with the correction for multiple
470 hypotheses by FDR-adjusted $p < 0.05$.
471
472 **Statistical analysis**
473 Statistical analyses were performed in GraphPad Prism using tests described in the Figure Legends.
474
475 **Reporting summary**
476 Further information on research design is available in the file Reporting Summary.
477
478 **Data availability**
479 All data needed to evaluate the conclusions in the paper are present in the file Combined Manuscript and
480 the file Supplementary Information.
481

ACKNOWLEDGMENTS

We thank Jingjing Wang at the Cell Biology Facility, Center of Biomedical Analysis, Tsinghua University, for help with confocal microscopy. We thank Meng Han in Protein Chemistry and proteomics Facility at Technology Center for Protein Sciences, Tsinghua University, for protein MS analysis. We thank Nathalie Balaban's lab at Racah Institute of Physics, The Hebrew University of Jerusalem, for providing the *E. coli* KLY strain. This work was supported by the National Key Research and Development Program of China (2022YFC2303202), the Tsinghua-Peking Joint Center for Life Sciences (20111770319), and the Tsinghua University Dushi Program (20251080040) to J. L.

AUTHOR CONTRIBUTIONS

J. L. mainly designed experiments, acquired funding, and revised the paper. F. W. designed and performed experiments, analyzed data, and wrote the paper. Y. Z. performed the genome editing experiments, helped with the analysis of clinical isolates, and revised the paper.

COMPETING INTERESTS

The authors declare no competing interests.

MATERIALS & CORRESPONDENCE

Further information and requests for resources and reagents should be directed to, and will be fulfilled by, the lead contact, Jia-Feng Liu (jfliu@mail.tsinghua.edu.cn).

SUPPLEMENTARY INFORMATION

The file Supplementary Information includes Extended Data Figs. 1–9 and Supplementary Tables 1–5.

507 **FIGURE TITLES AND LEGENDS**

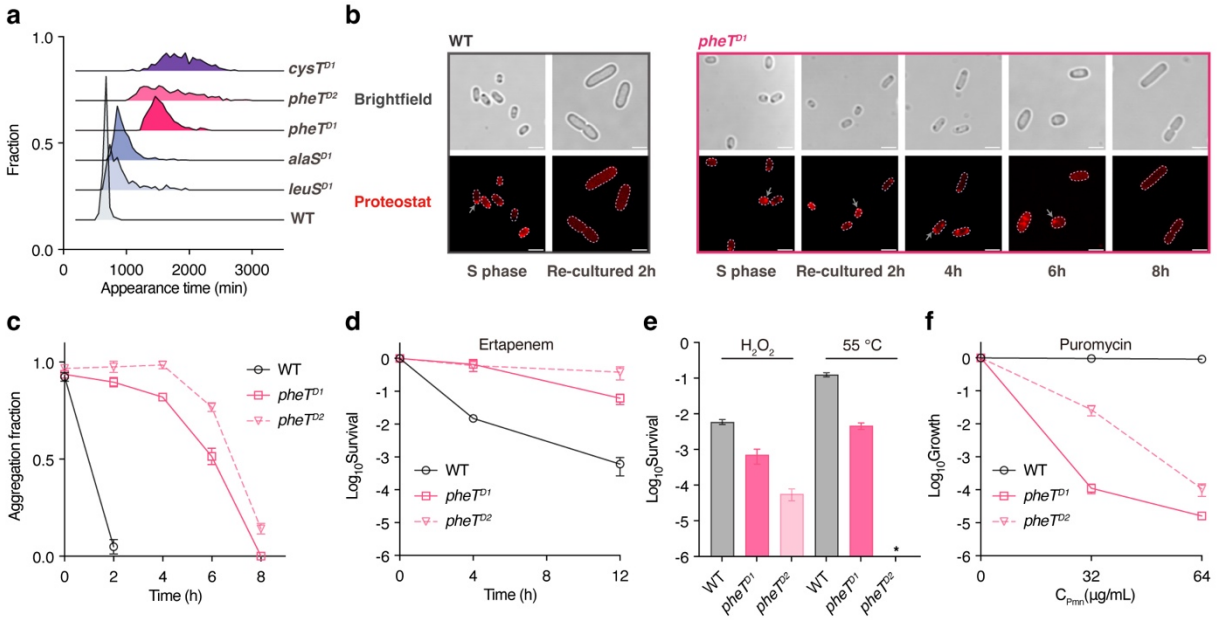

508 **Fig. 1. Delayed aggregate disassembly and increased vulnerability to proteotoxic stress in long-lag**
509 **mutants. a**, Appearance time distribution for WT and identified dormant mutants measured by ScanLag. **b**,
510 Representative brightfield and fluorescence images of WT and *pheT*^{D1} cells stained with Proteostat. Cells
511 from the stationary phase (S phase) were re-cultured in fresh LB medium and sampled at the indicated time
512 points. Arrows indicate Proteostat-positive aggregates. Scale bars, 2 μm. **c**, Quantification of the fraction
513 of WT, *pheT*^{D1}, and *pheT*^{D2} cells containing Proteostat-positive aggregates upon re-culturing in fresh LB
514 medium. Data are presented as mean ± SD (n = 4). **d**, Survival of WT, *pheT*^{D1}, and *pheT*^{D2} cells after 1
515 μg/mL ertapenem treatment for 4 h or 12 h. Data are presented as mean ± SD (n = 3). **e**, Survival of WT,
516 *pheT*^{D1}, and *pheT*^{D2} cells after oxidative stress (10 mM H_2O_2, 30 minutes) or heat shock (55 °C, 30 minutes).
517 Asterisk indicates values below detection limit (< 10^{-7}). Data are presented as mean ± SD (n = 3). **f**, Growth
518 fraction of WT, *pheT*^{D1}, and *pheT*^{D2} cells on solid medium containing the indicated concentrations of
519 puromycin relative to drug-free plates. Data are presented as mean ± SD (n = 3).

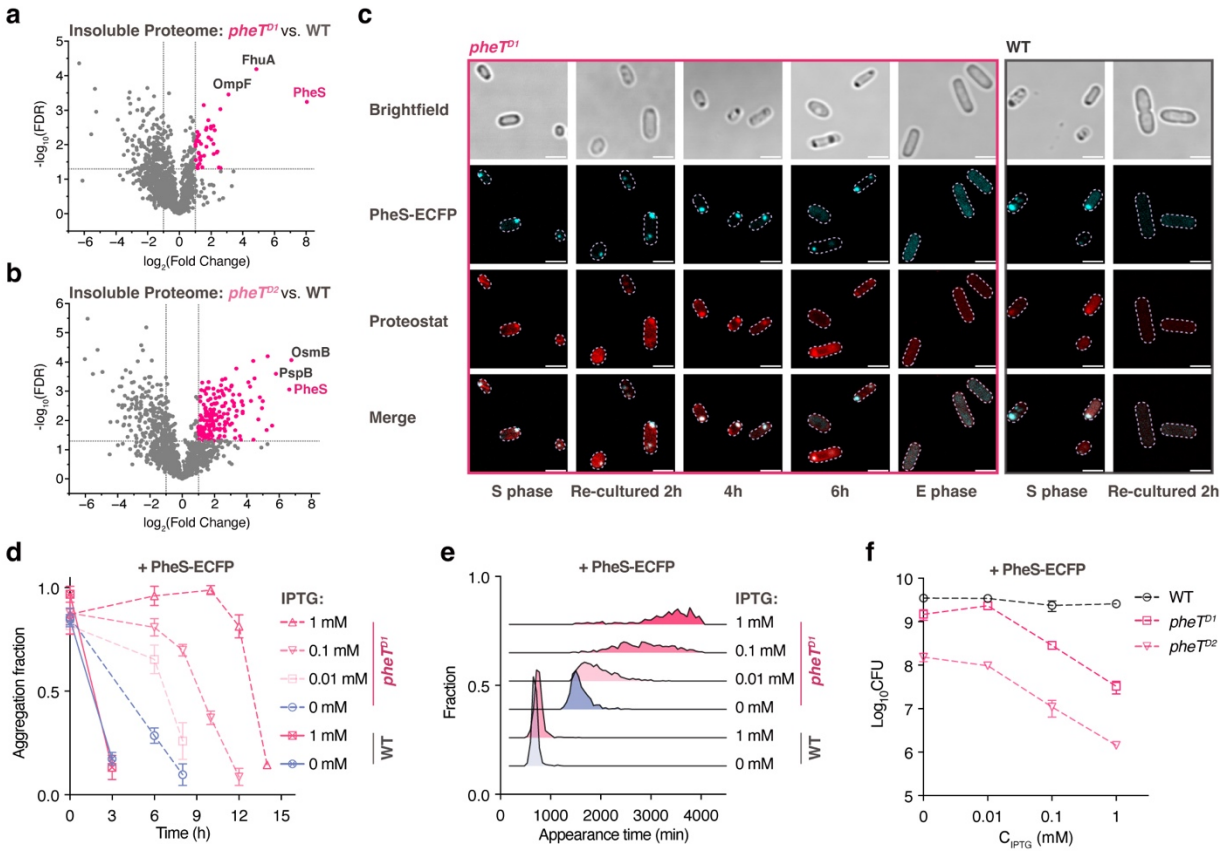

Fig. 2. Increased PheS aggregation delays aggregate disassembly and extends lag time. a,**b**, Volcano plots showing MS analysis of the insoluble proteome in *pheT*^{D1} and *pheT*^{D2} relative to WT at the stationary phase. Student's *t*-test with the correction to multiple hypotheses by FDR adjusted $p < 0.05$. n = 3 biological replicates. **c**, Representative brightfield and fluorescence images of WT and *pheT*^{D1} cells expressing ECFP-tagged PheS and stained with Proteostat. Cells from the stationary phase were re-cultured in fresh LB medium and stained with Proteostat at the indicated time points. Scale bars, 2 μm. **d**, Quantification of the fraction of WT and *pheT*^{D1} cells containing Proteostat-positive aggregates during recovery in fresh LB medium. Cells with the inducible expression of PheS-ECFP were grown for 48 hours at the indicated concentrations of IPTG, and then transferred to fresh LB medium for recovery. Data are presented as mean ± SD (n = 4). **e**, Appearance time distribution for WT and *pheT*^{D1} cells after the inducible expression of PheS-ECFP for 48 hours at the indicated concentrations of IPTG. **f**, CFU of WT, *pheT*^{D1}, and *pheT*^{D2} bacteria after the inducible expression of PheS-ECFP for 48 hours at the indicated concentrations of IPTG. Data are presented as mean ± SD (n = 3).

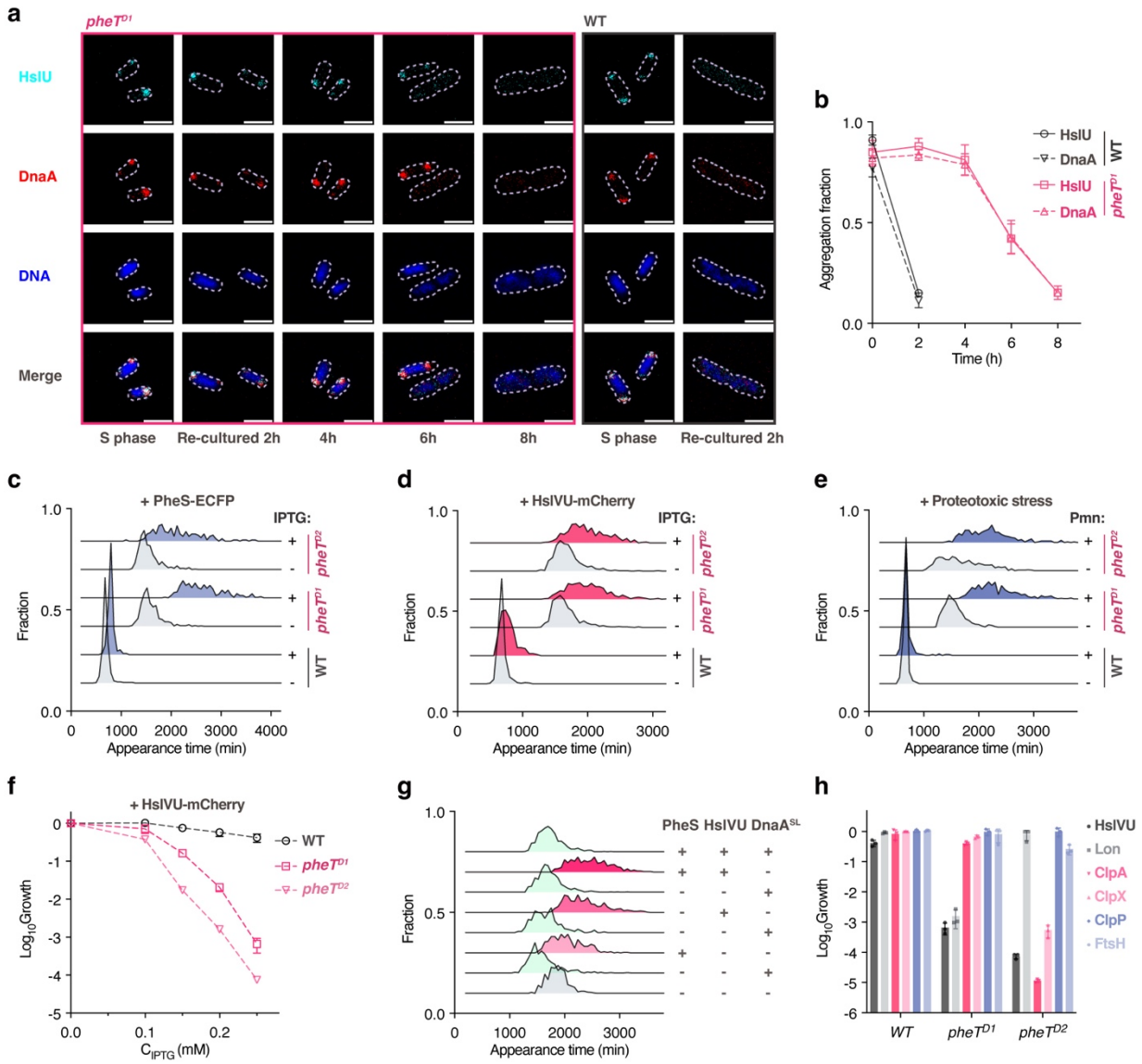

Fig. 3. Sequestration of the replication initiator DnaA within protein aggregates delays replication initiation. a, Fluorescence images of dual-labelled strains (chromosomally labelled HslU-ECFP and mCherry-DnaA) stained with DAPI upon re-culturing. Cells from the stationary phase were re-cultured in fresh LB medium and sampled at the indicated time points. Scale bars, 2 μm. **b**, Quantification of the fraction of WT and *pheT*^{D1} cells containing HslU-ECFP foci or mCherry-DnaA foci upon re-culturing. Data are presented as mean ± SD (n = 4). **c**–**e**, Appearance time distribution for WT, *pheT*^{D1}, and *pheT*^{D2} cells when incubated with the induced expression of PheS-ECFP (0.15 mM IPTG), HslVU-mCherry (0.25 mM IPTG), or puromycin (16 μg/mL). **f**, Growth fraction of WT, *pheT*^{D1}, and *pheT*^{D2} cells when incubated with the inducible expression of HslVU-mCherry at the indicated concentrations of IPTG relative to IPTG-free plates. Data are presented as mean ± SD (n = 3). **g**, Appearance time distribution for *pheT*^{D1} cells when incubated with the anhydrotetracycline-induced PheS (1 ng/mL anhydrotetracycline), arabinose-induced HslVU-ECFP (100 mM arabinose), or IPTG-inducible soluble DnaA-mCherry (0.25 mM IPTG). **h**, Growth fraction of WT, *pheT*^{D1}, and *pheT*^{D2} cells when incubated with the inducible expression of proteases (0.25 mM IPTG) relative to IPTG-free plates. Data are presented as mean ± SD (n = 3).

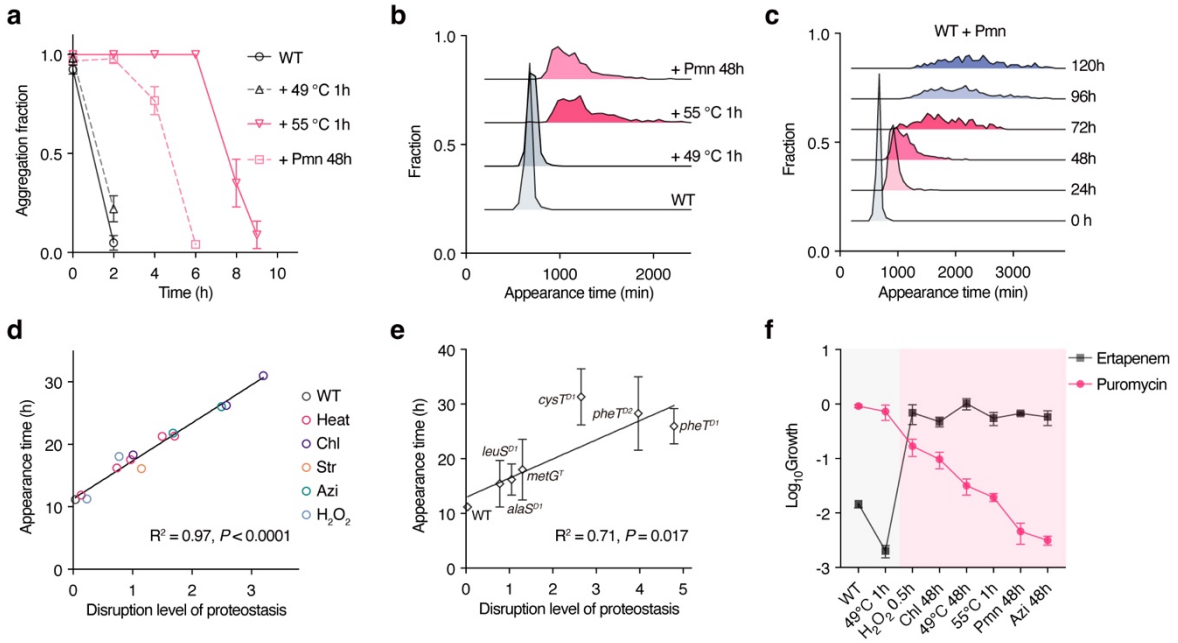

Fig. 4. Lag time scales with proteostasis disruption across stresses. a, Quantification of the fraction of stress-treated WT cells containing Proteostat-positive aggregates upon re-culturing. WT cells were treated with the indicated stress, and upon stress removal, bacteria were re-cultured with fresh LB medium and stained with Proteostat at the indicated time points. Data are presented as mean ± SD (n = 4). **b**, Appearance time distribution for WT after treatment with the indicated stress. **c**, Appearance time distribution for WT after exposure to 256 μg/mL puromycin for the indicated durations. **d**, Mean appearance time plotted against the disruption level of proteostasis after treatment with the indicated stress. Each point represents the mean of n = 3 biological replicates for each stress condition. The disruption level of proteostasis is quantified as the $\log_{10}$ ratio of CFU on antibiotic-free versus 64 μg/mL puromycin plates. From left to right: Heat: 49 °C for 1 h, 24 h, or 48 h; 55 °C for 0.5 h or 1 h; Chloramphenicol (Chl): 500 μg/mL for 48 h, 72 h, 96 h; Streptomycin (Str): 50 μg/mL for 2 h; Azithromycin (Azi): 100 μg/mL for 24 h, 48 h; H_2O_2: 5 mM or 10 mM for 0.5 h. The solid line denotes linear regression (R^2 = 0.97, P < 0.0001). **e**, Appearance time plotted against the disruption level of proteostasis for the identified dormant mutants. The disruption level of proteostasis is quantified as the $\log_{10}$ ratio of CFU on antibiotic-free versus 64 μg/mL puromycin plates. The solid line denotes linear regression (R^2 = 0.71, P = 0.017). Data are presented as mean ± SD (n = 3). **f**, Growth fraction of stress-treated WT cells on puromycin plates (64 μg/mL) relative to drug-free plates and survival after 4 h of 1 μg/mL ertapenem treatment. Data are presented as mean ± SD (n = 3).

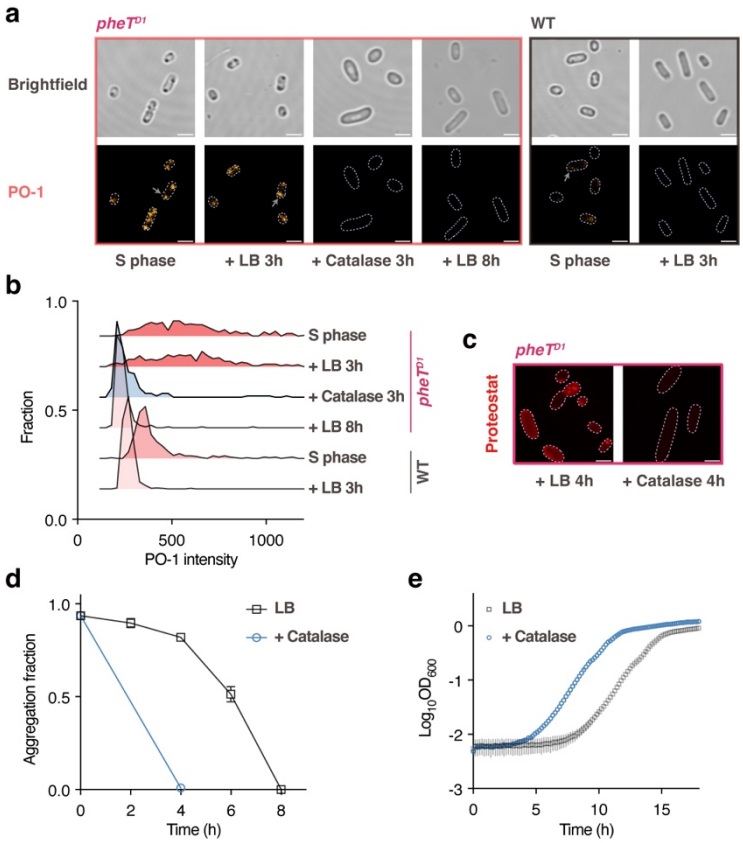

Fig. 5. Restoration of proteostasis promotes exit from dormancy. a, Representative brightfield and fluorescence images of WT and *pheT*^{D1} bacteria stained with Peroxy Orange 1 (PO-1). Cells from the stationary phase were re-cultured in LB or LB supplemented with 0.1 mg/mL catalase and sampled at the indicated time points. Arrows indicate PO-1-positive aggregates. Scale bars, 2 μm. **b**, PO-1 fluorescence intensity distribution for WT and *pheT*^{D1} cells at the indicated time points during recovery. **c**, Representative fluorescence images of *pheT*^{D1} bacteria stained with Proteostat after re-culturing in LB or LB supplemented with 0.1 mg/mL catalase. Scale bars, 2 μm. **d**, Quantification of the fraction of *pheT*^{D1} cells containing Proteostat-positive aggregates upon re-culturing in LB or LB supplemented with 0.1 mg/mL catalase. Data are presented as mean ± SD (n = 4). **e**, Growth curves of *pheT*^{D1} bacteria were monitored by measuring optical density at 600 nm (OD_{600}) over time in LB or LB supplemented with 0.1 mg/mL catalase. Data are presented as mean ± SD (n = 3).

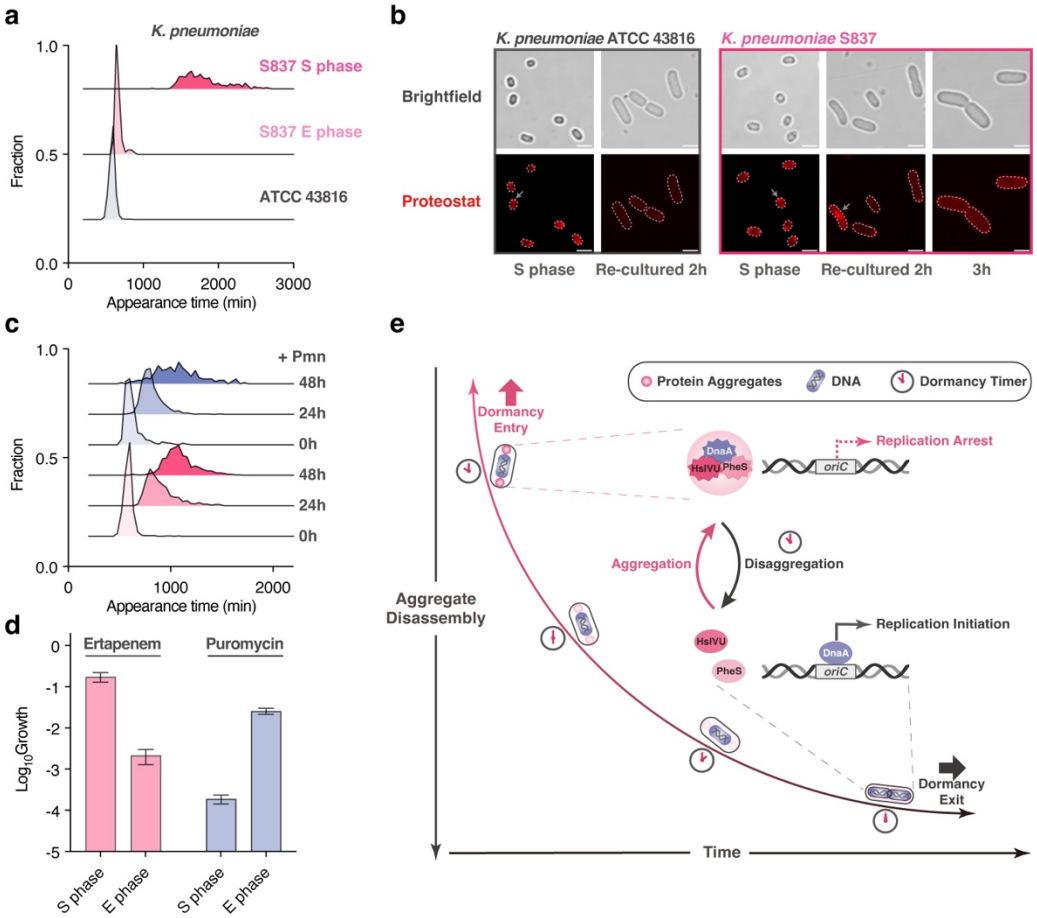

Fig. 6. Proteostasis-governed dormancy in clinical isolates. a, Appearance time distribution for clinical isolate *K. pneumoniae* S837 at the stationary phase (S phase) or exponential phase (E phase), and laboratory strain ATCC 43816 at the S phase. **b**, Representative brightfield and fluorescence images of *K. pneumoniae* ATCC 43816 and clinical *K. pneumoniae* S837 stained with Proteostat. Bacteria from the stationary phase were re-cultured in fresh LB medium and sampled at the indicated time points. Arrows indicate Proteostat-positive aggregates. Scale bars, 2 μm. **c**, Appearance time distribution for *K. pneumoniae* ATCC 43816 (bottom) and *B. subtilis* PY79 (upper) after 256 μg/mL puromycin exposure for the indicated durations. **d**, Growth fraction of S/E-phase *K. pneumoniae* S837 on puromycin plates (64 μg/mL) relative to drug-free plates and survival after 3 h of 1 μg/mL ertapenem treatment. Data are presented as mean ± SD (n = 3). **e**, Formation and disassembly of protein aggregates function as a timing device for bacterial dormancy. Upon entry into dormancy, protein aggregates, such as insoluble PheS, sequester the protease HslVU and the replication initiator DnaA away from the bacterial nucleoid, thereby preventing replication initiation. After nutrient replenishment, bacterial replication initiation remains inhibited until aggregates are disassembled, allowing DnaA to reassociate with the chromosomal origin of replication (*oriC*). The rate of aggregate disassembly thus determines the duration of bacterial dormancy.

595 **REFERENCES**

596 1 Jonas, K., Liu, J., Chien, P. & Laub, M. T. Proteotoxic stress induces a cell-cycle arrest by
597 stimulating Lon to degrade the replication initiator DnaA. *Cell* **154**, 623-636 (2013).
598 https://doi.org:10.1016/j.cell.2013.06.034
599 2 Fridman, O., Goldberg, A., Ronin, I., Shoresh, N. & Balaban, N. Q. Optimization of lag time
600 underlies antibiotic tolerance in evolved bacterial populations. *Nature* **513**, 418-421 (2014).
601 https://doi.org:10.1038/nature13469
602 3 Levin-Reisman, I. *et al.* Antibiotic tolerance facilitates the evolution of resistance. *Science* **355**,
603 826-830 (2017). https://doi.org:10.1126/science.aaj2191
604 4 Pu, Y. *et al.* ATP-Dependent Dynamic Protein Aggregation Regulates Bacterial Dormancy Depth
605 Critical for Antibiotic Tolerance. *Mol Cell* **73**, 143-156.e144 (2019).
606 https://doi.org:10.1016/j.molcel.2018.10.022
607 5 Blattman, S. B. *et al.* Identification and genetic dissection of convergent persister cell states.
608 *Nature* **636**, 438-446 (2024). https://doi.org:10.1038/s41586-024-08124-2
609 6 Liu, J., Gefen, O., Ronin, I., Bar-Meir, M. & Balaban, N. Q. Effect of tolerance on the evolution of
610 antibiotic resistance under drug combinations. *Science* **367**, 200-204 (2020).
611 https://doi.org:10.1126/science.aay3041
612 7 Balaban, N. Q., Merrin, J., Chait, R., Kowalik, L. & Leibler, S. Bacterial persistence as a phenotypic
613 switch. *Science* **305**, 1622-1625 (2004). https://doi.org:10.1126/science.1099390
614 8 Hansen, S., Lewis, K. & Vulić, M. Role of global regulators and nucleotide metabolism in
615 antibiotic tolerance in *Escherichia coli*. *Antimicrob Agents Chemother* **52**, 2718-2726 (2008).
616 https://doi.org:10.1128/aac.00144-08
617 9 Girgis, H. S., Harris, K. & Tavazoie, S. Large mutational target size for rapid emergence of
618 bacterial persistence. *Proc Natl Acad Sci U S A* **109**, 12740-12745 (2012).
619 https://doi.org:10.1073/pnas.1205124109
620 10 Yu, J., Liu, Y., Yin, H. & Chang, Z. Regrowth-delay body as a bacterial subcellular structure
621 marking multidrug-tolerant persisters. *Cell Discov* **5**, 8 (2019). https://doi.org:10.1038/s41421-
622 019-0080-3
623 11 Dewachter, L. *et al.* The Dynamic Transition of Persistence toward the Viable but Nonculturable
624 State during Stationary Phase Is Driven by Protein Aggregation. *mBio* **12**, e0070321 (2021).
625 https://doi.org:10.1128/mBio.00703-21
626 12 Bollen, C. *et al.* Composition and liquid-to-solid maturation of protein aggregates contribute to
627 bacterial dormancy development and recovery. *Nat Commun* **16**, 1046 (2025).
628 https://doi.org:10.1038/s41467-025-56387-8
629 13 Zhang, Z., Li, D., Zheng, B. & Liu, J. F. DEAD-box ATPase-marked condensates coordinate
630 compartmentalized translation and antibiotic persistence. *Sci Adv* **12**, eady1930 (2026).
631 https://doi.org:10.1126/sciadv.ady1930
632 14 Levin-Reisman, I. *et al.* Automated imaging with ScanLag reveals previously undetectable
633 bacterial growth phenotypes. *Nat Methods* **7**, 737-739 (2010).
634 https://doi.org:10.1038/nmeth.1485
635 15 Kaspy, I. *et al.* HipA-mediated antibiotic persistence via phosphorylation of the glutamyl-tRNA-
636 synthetase. *Nat Commun* **4**, 3001 (2013). https://doi.org:10.1038/ncomms4001
637 16 Shen, D. *et al.* Novel cell- and tissue-based assays for detecting misfolded and aggregated
638 protein accumulation within aggresomes and inclusion bodies. *Cell Biochem Biophys* **60**, 173-185
639 (2011). https://doi.org:10.1007/s12013-010-9138-4

640 17 Leeman, D. S. *et al.* Lysosome activation clears aggregates and enhances quiescent neural stem
641 cell activation during aging. *Science* **359**, 1277-1283 (2018).
642 https://doi.org:10.1126/science.aag3048
643 18 Tomoyasu, T., Mogk, A., Langen, H., Goloubinoff, P. & Bukau, B. Genetic dissection of the roles
644 of chaperones and proteases in protein folding and degradation in the *Escherichia coli* cytosol.
645 *Mol Microbiol* **40**, 397-413 (2001). https://doi.org:10.1046/j.1365-2958.2001.02383.x
646 19 Gidalevitz, T., Ben-Zvi, A., Ho, K. H., Brignull, H. R. & Morimoto, R. I. Progressive disruption of
647 cellular protein folding in models of polyglutamine diseases. *Science* **311**, 1471-1474 (2006).
648 https://doi.org:10.1126/science.1124514
649 20 Labbadia, J. & Morimoto, R. I. The biology of proteostasis in aging and disease. *Annu Rev*
650 *Biochem* **84**, 435-464 (2015). https://doi.org:10.1146/annurev-biochem-060614-033955
651 21 Hipp, M. S. & Hartl, F. U. Interplay of Proteostasis Capacity and Protein Aggregation: Implications
652 for Cellular Function and Disease. *J Mol Biol* **436**, 168615 (2024).
653 https://doi.org:10.1016/j.jmb.2024.168615
654 22 Mirzaei, H. & Regnier, F. Protein:protein aggregation induced by protein oxidation. *J Chromatogr*
655 *B Analyt Technol Biomed Life Sci* **873**, 8-14 (2008).
656 https://doi.org:10.1016/j.jchromb.2008.04.025
657 23 Brøndsted, L., Andersen, M. T., Parker, M., Jørgensen, K. & Ingmer, H. The HtrA protease of
658 *Campylobacter jejuni* is required for heat and oxygen tolerance and for optimal interaction with
659 human epithelial cells. *Appl Environ Microbiol* **71**, 3205-3212 (2005).
660 https://doi.org:10.1128/aem.71.6.3205-3212.2005
661 24 Servant, P. *et al.* The ClpPX protease is required for radioresistance and regulates cell division
662 after gamma-irradiation in *Deinococcus radiodurans*. *Mol Microbiol* **66**, 1231-1239 (2007).
663 https://doi.org:10.1111/j.1365-2958.2007.06003.x
664 25 Mermershtain, I. *et al.* Idiosyncrasy and identity in the prokaryotic Phe-system: crystal structure
665 of *E. coli* phenylalanyl-tRNA synthetase complexed with phenylalanine and AMP. *Protein Sci* **20**,
666 160-167 (2011). https://doi.org:10.1002/pro.549
667 26 Mahmoud, S. A. & Chien, P. Regulated Proteolysis in Bacteria. *Annu Rev Biochem* **87**, 677-696
668 (2018). https://doi.org:10.1146/annurev-biochem-062917-012848
669 27 Joshi, K. K. & Chien, P. Regulated Proteolysis in Bacteria: *Caulobacter*. *Annu Rev Genet* **50**, 423-
670 445 (2016). https://doi.org:10.1146/annurev-genet-120215-035235
671 28 Gross, M. H. & Konieczny, I. Polyphosphate induces the proteolysis of ADP-bound fraction of
672 initiator to inhibit DNA replication initiation upon stress in *Escherichia coli*. *Nucleic Acids Res* **48**,
673 5457-5466 (2020). https://doi.org:10.1093/nar/gkaa217
674 29 Gbolahan, A. *et al.* A novel membrane stress response that blocks chromosomal replication by
675 targeting the DnaA initiator via the ClpP protease. *J Bacteriol* **207**, e0015125 (2025).
676 https://doi.org:10.1128/jb.00151-25
677 30 Winkler, J. *et al.* Quantitative and spatio-temporal features of protein aggregation in *Escherichia*
678 *coli* and consequences on protein quality control and cellular ageing. *Embo j* **29**, 910-923 (2010).
679 https://doi.org:10.1038/emboj.2009.412
680 31 Coquel, A. S. *et al.* Localization of protein aggregation in *Escherichia coli* is governed by diffusion
681 and nucleoid macromolecular crowding effect. *PLoS Comput Biol* **9**, e1003038 (2013).
682 https://doi.org:10.1371/journal.pcbi.1003038
683 32 Ayrapetyan, M., Williams, T. C. & Oliver, J. D. Bridging the gap between viable but non-
684 culturable and antibiotic persistent bacteria. *Trends Microbiol* **23**, 7-13 (2015).
685 https://doi.org:10.1016/j.tim.2014.09.004

686 33 Nozaki, S., Niki, H. & Ogawa, T. Replication initiator DnaA of *Escherichia coli* changes its assembly
687 form on the replication origin during the cell cycle. *J Bacteriol* **191**, 4807-4814 (2009).
688 https://doi.org:10.1128/jb.00435-09
689 34 Boeneman, K. *et al. Escherichia coli* DnaA forms helical structures along the longitudinal cell axis
690 distinct from MreB filaments. *Mol Microbiol* **72**, 645-657 (2009). https://doi.org:10.1111/j.1365-
691 2958.2009.06674.x
692 35 Ferguson, A. D., Hofmann, E., Coulton, J. W., Diederichs, K. & Welte, W. Siderophore-mediated
693 iron transport: crystal structure of FhuA with bound lipopolysaccharide. *Science* **282**, 2215-2220
694 (1998). https://doi.org:10.1126/science.282.5397.2215
695 36 Killmann, H., Herrmann, C., Wolff, H. & Braun, V. Identification of a new site for ferrichrome
696 transport by comparison of the FhuA proteins of *Escherichia coli*, *Salmonella paratyphi* B,
697 *Salmonella typhimurium*, and *Pantoea agglomerans*. *J Bacteriol* **180**, 3845-3852 (1998).
698 https://doi.org:10.1128/jb.180.15.3845-3852.1998
699 37 Dai, Y. *et al.* Interface of biomolecular condensates modulates redox reactions. *Chem* **9**, 1594-
700 1609 (2023). https://doi.org:10.1016/j.chempr.2023.04.001
701 38 Chen, M. W. *et al.* Transition-State-Dependent Spontaneous Generation of Reactive Oxygen
702 Species by Aβ Assemblies Encodes a Self-Regulated Positive Feedback Loop for Aggregate
703 Formation. *J Am Chem Soc* **147**, 8267-8279 (2025). https://doi.org:10.1021/jacs.4c15532
704 39 Dickinson, B. C., Huynh, C. & Chang, C. J. A palette of fluorescent probes with varying emission
705 colors for imaging hydrogen peroxide signaling in living cells. *J Am Chem Soc* **132**, 5906-5915
706 (2010). https://doi.org:10.1021/ja1014103
707 40 Lippert, A. R., Van de Bittner, G. C. & Chang, C. J. Boronate oxidation as a bioorthogonal reaction
708 approach for studying the chemistry of hydrogen peroxide in living systems. *Acc Chem Res* **44**,
709 793-804 (2011). https://doi.org:10.1021/ar200126t
710 41 Py, B. & Barras, F. Building Fe-S proteins: bacterial strategies. *Nat Rev Microbiol* **8**, 436-446
711 (2010). https://doi.org:10.1038/nrmicro2356
712 42 Alfonso-Prieto, M., Biarnés, X., Vidossich, P. & Rovira, C. The molecular mechanism of the
713 catalase reaction. *J Am Chem Soc* **131**, 11751-11761 (2009). https://doi.org:10.1021/ja9018572
714 43 Kohanski, M. A., Dwyer, D. J., Hayete, B., Lawrence, C. A. & Collins, J. J. A common mechanism of
715 cellular death induced by bactericidal antibiotics. *Cell* **130**, 797-810 (2007).
716 https://doi.org:10.1016/j.cell.2007.06.049
717 44 Alberti, S. & Hyman, A. A. Biomolecular condensates at the nexus of cellular stress, protein
718 aggregation disease and ageing. *Nature Reviews Molecular Cell Biology* **22**, 196-213 (2021).
719 https://doi.org:10.1038/s41580-020-00326-6
720 45 Zhang, E. E. & Kay, S. A. Clocks not winding down: unravelling circadian networks. *Nat Rev Mol*
721 *Cell Biol* **11**, 764-776 (2010). https://doi.org:10.1038/nrm2995
722 46 Bollen, C., Dewachter, L. & Michiels, J. Protein Aggregation as a Bacterial Strategy to Survive
723 Antibiotic Treatment. *Front Mol Biosci* **8**, 669664 (2021).
724 https://doi.org:10.3389/fmolb.2021.669664
725 47 Schramm, F. D., Schroeder, K. & Jonas, K. Protein aggregation in bacteria. *FEMS Microbiol Rev*
726 **44**, 54-72 (2020). https://doi.org:10.1093/femsre/fuz026
727 48 Saad, S. *et al.* Reversible protein aggregation is a protective mechanism to ensure cell cycle
728 restart after stress. *Nat Cell Biol* **19**, 1202-1213 (2017). https://doi.org:10.1038/ncb3600
729 49 Zaffagnini, G. *et al.* Mouse oocytes sequester aggregated proteins in degradative super-
730 organelles. *Cell* **187**, 1109-1126.e1121 (2024). https://doi.org:10.1016/j.cell.2024.01.031
731 50 Audas, T. E. *et al.* Adaptation to Stressors by Systemic Protein Amyloidogenesis. *Dev Cell* **39**,
732 155-168 (2016). https://doi.org:10.1016/j.devcel.2016.09.002

733 51 Rosswag de Souza, S., Böke, E. & Zaffagnini, G. Proteostasis in cellular dormancy: lessons from
734 yeast to oocytes. *Trends Biochem Sci* **50**, 646-662 (2025).
735 https://doi.org:10.1016/j.tibs.2025.05.004
736 52 Thomason, L. C., Costantino, N. & Court, D. L. *E. coli* genome manipulation by P1 transduction.
737 *Curr Protoc Mol Biol* **Chapter 1**, 1.17.11-11.17.18 (2007).
738 https://doi.org:10.1002/0471142727.mb0117s79
739 53 Näsvall, J., Knöppel, A. & Andersson, D. I. Duplication-Insertion Recombineering: a fast and scar-
740 free method for efficient transfer of multiple mutations in bacteria. *Nucleic Acids Res* **45**, e33
741 (2017). https://doi.org:10.1093/nar/gkw1078

742